A thesis for the Degree of Bachelor of Science (Hons)

Optical Autocorrelation using Non-Linearity in a Simple Photodiode

Syed Abdullah Aljunid

Supervisor: Assistant Professor Antia Lamas-Linares

Department of Physics
National University of Singapore
2006/2007

Abstract

We report on the development and characterisation of an intensity autocorrelator for measuring short femtosecond pulses using non-linearity of a light emitting diode (LED). In this thesis, we concentrate in particular into the requirements for an intensity autocorrelator, especially the non-linear detection process and why an LED makes a reasonable choice. An autocorrelator using a modified Mach-Zender interferometer setup with an LED as a non-linear detector was built and used to measure pulses from a mode-locked laser. Results of the measurements are presented for pulses of various widths from 130 fs up to 5.7 ps. Dispersion through an optical fiber is also examined and further possibilities suggested.

Acknowledgements

I would like to thank Asst. Prof Antia Lamas-Linares for her continuous support, motivation and advice throughout my entire project.

Also, many thanks to Assoc. Prof Christian Kurtsiefer for giving me the opportunity to work in the Quantum Information Technology (QIT) Group. Finally everyone else in the Quantum Optics Group of QIT, for never failing to answer questions, for helping me with any difficulties I had and for not minding me as I hang around in the lab longer than I had to, looking curiously at all the experimental setups.

Contents

Introduction

The field of ultrashort sciences is one that is getting very much attention in recent years. Many fundamental biological, chemical and physical processes occur in a time scale that is much less than that we are used to in everyday life. For example, photosynthesis, protein-folding and molecular vibrations all occur on a femtosecond time scale.

If we want to measure such processes in time, a much shorter event is needed so that we can resolve those processes temporally, much like how a strobe light is used in split-second photography. The ultrashort event required can be in the form of light pulses as short as femtoseconds or even attoseconds long in time. These ultrashort laser pulses can be readily generated in most labs using commercial mode-locked lasers together with a pulse compressor. Besides the temporal resolution, these pulses also have high intensities. A 100 fs pulse with 1 mJ of energy can yield intensities as high as 10^{16} W/cm^2. At such intensities, non-linear effects become more apparent which then leads to easier observations of such phenomena.

To determine accurately how short the generated pulses are, is not a trivial matter. We cannot measure them directly since there are no shorter events readily available, and even if there is, the problem just reduces to measuring that shorter event. Hence we will use the pulse to measure itself in a technique called autocorrelation. We shall also see that for an intensity

autocorrelation to be implemented experimentally a non-linear medium, such as a non-linear crystal, is required. It has been shown in [1, 2] that semiconductor photodiodes and light emitting diodes can be also used for non-linear detection of light.

The advantages of using semiconductor over non-linear crystals, besides its cheap price, is that we do not need to fulfill phase-matching conditions. Also there are no polarisation requirements by the semiconductor detectors. Both polarisation and phase-matching however, are important considerations in non-linear crystals. This can allow for a larger bandwidth of detectable non-linear effects, which is usually limited by the strict phase-matching requirements in non-linear crystals.

The light emitting diode will be looked at for its suitability and its design carefully examined. Since it is not designed for light detection, there are several challenges that we will face.

But first, we will begin by looking at how an autocorrelator works, that is, the theory of autocorrelation and how it can be implemented optically. Also , we will discuss how the actual pulse width is obtained from an autocorrelation.

Chapter 1

Autocorrelator

An autocorrelator is a device that compares a signal with a displaced copy itself. The output is the autocorrelation of the input signal, or some function of that signal.

1.1 Theory of autocorrelation

Mathematically, the cross-correlation of two complex square integrable functions, $f(x)$ and $g(x)$ is defined as,

$$(f \star g)(x) \equiv \int_{-\infty}^{\infty} f^*(t)g(x+t)\,dt, \tag{1.1}$$

where f^* is the complex conjugate of f. It is a measure of how similar the two functions are for different values of x. Completely uncorrelated functions will have a cross-correlation of zero for all x. On the other extreme, if $g(x) = f(x)$, then it just becomes a cross-correlation of f with itself, also called the autocorrelation of f, $A_f(x)$. The autocorrelation of a function

describe how similar a function is with a time-delayed copy itself.

$$\begin{aligned} A_f(x) &= \int_{-\infty}^{\infty} f^*(t) f(x+t)\, dt \\ &= \int_{-\infty}^{\infty} f^*(t-x) f(t)\, dt \end{aligned} \tag{1.2}$$

The autocorrelation of a function has several properties which we will be using later on and they are:

- It has a symmetry.
- There is a maximum at $x = 0$.
- If $f(x)$ is a periodic function, then $A_f(x)$ is also periodic with the same period.
- The autocorrelation of the sum of two functions, $A_h(x)$, where $h(x) = f(x) + g(x)$, is the sum of the two autocorrelations separately plus the cross-correlations of the two function.

An autocorrelation always has some symmetry. For real functions, where $f^* = f$, the symmetry is about $x = 0$. This can be seen easily from equation 1.2.

$$A_f(-x) = \int_{-\infty}^{\infty} f(t-(-x)) f(t)\, dt = \int_{-\infty}^{\infty} f(t+x) f(t)\, dt = A_f(x).$$

As such $A_f(x)$ is an even function.

At $x = 0$, we have

$$A_f(x=0) = \int_{-\infty}^{\infty} |f(t)|^2\, dt.$$

This is the maximum possible value of for $A_f(x)$ as a result of the Cauchy-Schwarz inequality. Hence for any autocorrelation we always have the maximum at $x = 0$.

If $f(x)$ is periodic, such that,

$$f(x + 2n\pi x_0) = f(x)$$

where x_0 is the period or wavelength of the function and n is a positive integer, the autocorrelation will also be periodic with the form,

$$A_f(x + 2n\pi x_0) = A_f(x).$$

For a function $h(x) = f(x) + g(x)$, its autocorrelation will be,

$$\begin{aligned} A_h(x) &= \int_{-\infty}^{\infty} h^*(t-x)h(t)\,dt \\ &= \int_{-\infty}^{\infty} \left[f^*(t-x) + g^*(t-x)\right]\left[f(t) + g(t)\right]\,dt \\ &= \int_{-\infty}^{\infty} f^*(t-x)f(t) + g^*(t-x)g(t) + f^*(t-x)g(t) + g^*(t-x)f(t)\,dt \\ &= A_f(x) + A_g(x) + (f \star g)(x) + (g \star f)(x), \end{aligned}$$

which is the sum of its components individual autocorrelation and cross-correlation terms. If the f and g are completely uncorrelated, their cross-correlation would be zero and $A_h(x)$ reduces to,

$$A_h(x) = A_f(x) + A_g(x).$$

The autocorrelation discards any phase term and returns only the magnitude squared of the function, evident in the $f(t)f^*(t + x)$ term. As such, it is a non-reversible operation. It means that for a given autocorrelation, without any additional information, we cannot infer the original function.

1.2 Electric field

Light is described by the electric field, $\mathbf{E}(\mathbf{r}, t)$, which is a function of both space and time. Since we are interested in its temporal properties, we simply

consider its time dependence. In most practical cases, it is convenient to write the electric field as the product of an amplitude function and a phase term. If the complex notation is employed, it can now be written as

$$E(t) = \mathcal{E}(t)e^{i(\omega_0+\phi(t))} + \text{c.c.} \tag{1.3}$$

where c.c. denotes complex conjugate, ω_0 is the carrier frequency of light, $\mathcal{E}(t)$ is the electric field amplitude of the light and $\phi(t)$ its time dependent phases. If the field envelope and time dependent phase terms are slow varying functions compared with the period of the carrier frequency, we can describe the light satisfactorily by these two terms. Intensity of the electric field is

$$I(t) = \frac{1}{2}\epsilon_0 cn\mathcal{E}(t)\mathcal{E}^*(t) \propto |\mathcal{E}(t)|^2$$

where the physical constants are usually ignored. For a pulse of light, the pulse duration, τ_p, is usually taken as the full width half maximum (FWHM) of the intensity profile.

The electric field can also be written in the frequency domain where its related by the Fourier transform. In the frequency domain,

$$E(\Omega) = \mathcal{E}(\Omega)e^{i\Phi(\Omega)}$$

where we don't write its complex conjugate terms anymore. The Fourier transform of the intensity is the spectral intensity,

$$S(\Omega) \propto |\mathcal{E}(\Omega)|^2$$

Similar to the pulse duration, the spectral width, $\Delta\omega_p$, is the FWHM of the spectral intensity profile. The pulse duration-bandwidth product is

$$\tau_p \Delta\omega_p \geq 2\pi K \tag{1.4}$$

Field envelope	Intensity profile	τ_p (FWHM)	Spectral profile	$\Delta\omega_p$ (FWHM)	$K = \tau_p \Delta\omega_p / 2\pi$
Gaussian	e^{-2t^2}	1.177	$e^{-(\pi\Omega)^2/2}$	2.355	0.441
Sech	$\text{sech}^2(t)$	1.763	$\text{sech}^2(\pi\Omega/2)$	1.122	0.315
Square	1 for $\lvert t\rvert \leq \frac{1}{2}$ 0 elsewhere	1	$\text{sinc}^2(\Omega)$	2.78	0.443

TABLE 1.1: Examples of standard pulse profiles [3, 4].

where K is a numerical constant depending on the actual pulse shape. Values for common field envelopes are given in table 1.1. For a pulse where there are no phase variations, called a bandwidth limited or Fourier transform limited pulse, the expression is reduced to an equality.

The electric field obeys the superposition principle,

$$E(t) = E_1(t) + E_2(t). \tag{1.5}$$

This will be exploited later on to get terms proportional to $E_1 \cdot E_2$. There are many more properties of the electric field, but this is sufficient to describe what we'll be doing.

Field envelopes

For a pulse of light, it is necessary that the electric field be non-zero only for a limited time and be zero at other times. In essence, the amplitude term in equation 1.3 must have a form that satisfy this condition. Since, $\mathcal{E}$ envelopes the oscillating electric field, it is also referred to as the field envelope.

Typical analytical envelope functions are the Gaussian and the hyperbolic secant, which arises when solving Maxwell's equations with a particular set of boundary conditions. In a mode-locked laser, which is the system that we'll be using to perform our experiments, it was shown [5] that a stationary solution has the form,

$$\mathcal{E}(t) \propto \operatorname{sech}(t).$$

This solution describes a stable pulse in an optical soliton that does not experience any changes to its electric field amplitude or phase.

1.3 Optical Autocorrelation

There are various forms of autocorrelation in optics depending on what is being measured. Each of these autocorrelations can be realised experimentally by using suitable optical elements. The simplest optical autocorrelation is that of the *field autocorrelation* where the electric field, E, is what we are interested in. The electric field is a function of time and so we write its autocorrelation as,

$$A^{(1)}(\tau) = \int_{-\infty}^{\infty} E(t)E^*(t-\tau)\,dt$$

where τ is the delay introduced. A field autocorrelation is also referred to as a first order autocorrelation. It is related to the spectrum by a Fourier transform

$$S(\Omega) = \mathcal{F}\left\{A^{(1)}\right\}$$

The *intensity autocorrelation*, $A_c(\tau)$, can also be measured experimentally.

$$A_c(\tau) = \int_{-\infty}^{\infty} I(t)I(t-\tau)\,dt = A^{(2)}(\tau) \tag{1.6}$$

The intensity autocorrelation is commonly referred to as the second order autocorrelation. Higher order correlations for intensity are also possible in which case the definition differs slightly,

$$A^{(n)}(\tau) = \int_{-\infty}^{\infty} I(t) I^n(t-\tau)\, dt.$$

For a reasonably peaked function, and a large enough n, I^n behaves like a delta function, $\delta(t)$. A cross-correlation of any function with a delta function is simply the function itself and hence the shape of $A^{(n)}$ is the same as the shape of the pulse.

Determining the pulse width from the intensity autocorrelation, $A_c(\tau)$, requires some previous knowledge of the pulse shape. If a pulse shape is assumed, the autocorrelation width, τ_{ac}, is related to the pulse width, τ_p, by some deconvolution factor, k.

$$\tau_{ac} = k\tau_p \tag{1.7}$$

The deconvolution factor can be calculated for analytical pulse shapes or computed numerically for complicated pulses. Table 1.2 lists deconvolution factors for some common pulse shapes.

1.4 Autocorrelation signals

An autocorrelator can be made such that it gives purely the autocorrelation signal. More often than not though, the output of it is the sum of several terms, one of which is the autocorrelation. This is because of the way the cross term in the autocorrelation is generated and detected. An autocorrelator is just a device that splits a light pulse into two, varies the delay in one and then combines them back. A detector sensitive to the required au-

Pulse shape	$A_c(\tau)$	τ_{ac}	$k = \tau_{ac}/\tau_p$	$I_2(\tau) - (1 + 3A_c(\tau))$
Gaussian	$e^{-\tau^2}$	1.664	1.414	$\pm 4e^{(3\tau^2/4)}$
Sech	$\frac{3(\tau\cosh\tau - \sinh\tau)}{\sinh^3\tau}$	2.720	1.543	$\pm\frac{3[\sinh(2\tau)-2\tau]}{\sinh^3\tau}$
Square	$1 - \lvert\tau\rvert \quad \lvert\tau\rvert \leq 1$ $0 \quad$ elsewhere	1	1	$\pm 4(1 - \lvert\tau\rvert) \quad \lvert\tau\rvert \leq 1$ $0 \quad$ elsewhere

TABLE 1.2: Autocorrelation functions for some pulse shapes. The last column gives the extra terms in the envelopes of I_2 which are not necessarily proportional to A_c [6].

tocorrelation term is then placed at the output. The detector is usually slow enough such that it integrates over the whole pulse.

If a lot of identical pulses are available, the autocorrelation signal can be reconstructed from by varying the delay and taking measurements at each delay, making use of the periodicity property of the autocorrelation[1].

However, a typical detector, at optical frequencies, is usually only sensitive to the intensity, $I \propto |E|^2$ of the light. If $E(t)$ is a superposition of two

[1]There are also single-shot autocorrelators that samples the various time delay using just one pulse by overlapping the pulse at an angle such that different parts of the pulse moves through different amount of delay. A linear-array detector is then needed since all the delays are measured simultaneously.

electric fields, then from equation 1.5, if $E_2 = E_1$, we get,

$$\begin{aligned} I_1(\tau) &= \int_{-\infty}^{\infty} |E_1(t) + E_1(t-\tau)|^2 \, dt \\ &= \int_{-\infty}^{\infty} |E_1(t)|^2 + |E_1(t-\tau)|^2 \, dt \\ &+ \int_{-\infty}^{\infty} E_1(t)E_1^*(t-\tau) + E_1^*(t)E_1(t-\tau) \, dt \\ &= 2\int_{-\infty}^{\infty} |E_1(t)|^2 \, dt \\ &+ 2\int_{-\infty}^{\infty} Re[E_1(t)E_1^*(t-\tau)] \, dt. \\ &\propto 1 + A^{(1)}(\tau) \end{aligned} \tag{1.8}$$

The first term of equation 1.8 is a constant and the second term is the field autocorrelation, $A^{(1)}(\tau)$. Therefore if a detector which is only sensitive to intensity is placed at the output, it will measure a field autocorrelation signal on top of a background with a peak to background ratio of 2:1 as can be seen by setting τ to zero. The maximum always occurs at zero delay as mentioned earlier.

To measure higher order autocorrelations, we either need a detector that is able to detect the relevant correlation term or place an optical element that is able to generate that required term. With both methods, it can be seen that what is required is something that gives a non-linear response to the electric field.

For the intensity autocorrelation, let's say we are somehow able to detect the term $|E^2|^2$ directly which is not unreasonable since its just I^2. Then if the electric field is again a superposition of two time delayed electric fields

we get,

$$
\begin{aligned}
I_2(\tau) &= \int_{-\infty}^{\infty} \left|[E_1(t) + E_1(t-\tau)]^2\right|^2 \, dt \qquad (1.9)\\
&= \int_{-\infty}^{\infty} \left|E_1^2(t) + 2E_1(t)E_1(t-\tau) + E_1^2(t-\tau)\right|^2 \, dt \\
&= 2\int_{-\infty}^{\infty} I(t)^2 \, dt \\
&+ 4\int_{-\infty}^{\infty} I(t)I(t-\tau) \, dt \\
&+ 4\int_{-\infty}^{\infty} [I(t) + I(t-\tau)]Re[E_1(t)E_1^*(t-\tau)] \, dt \\
&+ 2\int_{-\infty}^{\infty} Re[{E_1}^2(t){E_1^*}^2(t-\tau)] \, dt \qquad (1.10)
\end{aligned}
$$

As can be seen, the second term in the expansion is just the intensity autocorrelation. The first integral term is a constant. The third term is the slightly modified version of the field autocorrelation introduced earlier. And the last term is the interferogram of the 2nd harmonic of $E(t)$, i.e. interference fringes at twice the frequency of that for $E(t)$. Since the signal measured, I_2 contains the intensity autocorrelation with fringes present, it is also referred to as the *fringe-resolved autocorrelation* (FRAC). It has a peak to background ratio of 8:1 as seen in figure 1.1.

Looking at equation 1.10 once again, we see that the last two terms have the form of

$$Re[f_1(t)f_2^*(t-\Theta)] \propto Re[e^{i\Theta}] \propto \cos\Theta$$

which has fast oscillating components compared with the other terms. If we are able to remove these two terms, either by averaging or making f_1 and f_2 orthogonal such that

$$\int_{-\infty}^{\infty} Re[f_1(t)f_2^*(t-\tau)] = 0$$

for all τ, we are only left with the first two terms. Let us call this new signal

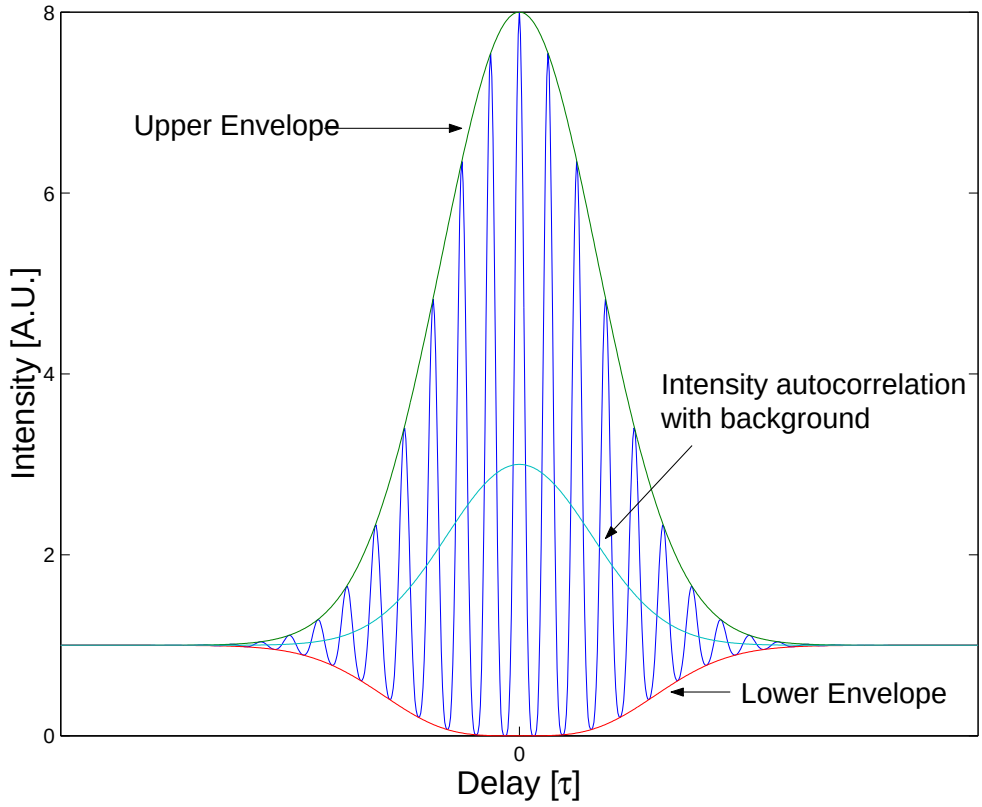

FIGURE 1.1: FRAC trace for a Gaussian pulse shape and its fringe resolved intensity autocorrelation signal.

$\tilde{I}_2$. So we have,

$$\begin{aligned} \tilde{I}_2(\tau) &= 2\int_{-\infty}^{\infty} I(t)^2\,dt \\ &\quad +4\int_{-\infty}^{\infty} I(t)I(t-\tau)\,dt \\ &\propto 1+2A_c(\tau) \end{aligned} \tag{1.11}$$

which is just the intensity autocorrelation sitting on top of a background with a peak to background ratio of 3:1 (see figure 1.1). This is similar to the autocorrelation of the sum of two uncorrelated functions but with an extra background term.

Chapter 2

Alternatives for non-linear medium

As we have seen in the previous chapter, in order to realise an intensity autocorrelation experimentally, we need a non-linear optical element or a detector that has non-linear response. There are a variety of elements and choices available each with its own merits and disadvantages.

Since the lowest order non-linear response is that for the second order, which is also the easiest to implement, we'll be looking for media with a second-order response to light. If we take the induced polarisation, $\mathcal{P}$, as a measure of its response, then we can write it as a function of the real electric field, $\mathcal{E}$, as follows,

$$\mathcal{P} = \varepsilon_0 \left[\chi^{(1)} E + \chi^{(2)} E^2 + \chi^{(3)} E^3 + \cdots \right]$$

where $\chi^{(1)}$, $\chi^{(2)}$ and $\chi^{(3)}$ are the first-, second- and third-order susceptibilities, tensors which measure how much a medium responds to the corresponding electric field terms.

2.1 Second order response

Most media already have some sort of non-linear response to light. However, this non-linear response is weak most of the time and thus drowned out by its linear response. Hence an important factor in choosing a suitable medium is a high non-linear susceptibility or, linear and non-linear responses that can be easily separated such that detection of the non-linear variety becomes possible.

Common methods for second order detection include detection of doubled frequency light from a second harmonic generation crystal [7], detection of light from two photon fluorescence [8], detection of transmitted light after two photon absorption [9] and detection of photocurrent generated by two photon absorption [1]. For each of these processes there is common need for a large electric field such that the non-linear effects becomes appreciable. This fits nicely with the measurement of short pulses since these short pulses typically have very higher peak intensities.

Second harmonic generation

A second harmonic generation (SHG) crystal can generate light at twice the frequency of the incident light. This can be loosely described as the destruction of two photons of lower energy to create a single photon with twice the energy. There are certain conditions that must be met for this generation to be efficient. The most important condition is phase matching. When this condition is met, the frequency doubled light generated throughout the crystal is in phase with each other, adding up constructively and thus giving a high doubling efficiency. For phase matching to be possible we need a crystal whose refractive indexes are the same at the fundamental frequency, ω and

double that frequency, 2ω,

$$n(\omega) = n(2\omega) \tag{2.1}$$

However, most normal crystals have refractive index that are monotonously increasing functions of frequency. Hence, phase matching is usually achieved by using a birefringent crystal where the refractive index depends on the polarisation of the light. For orthogonally polarised light, the ordinary and extraordinary indexes of refraction, n_o and n_e can be made to satisfy the above relation by choosing a suitable direction of propagation. In a positive crystal (e.g. quartz) $n_e > n_o$, so that equation 2.1 becomes

$$n_e(\omega) = n_o(2\omega)$$

There are two types of phase matching. In Type I phase matching, the two incident photons have the same polarisation while in Type II, they have orthogonal polarisation. Type II phase matching is frequently used in background and fringes free setups. A high-pass filter is placed at the output to separate the frequency-doubled light which is then detected by a normal photodetector or photomultiplier. Besides direction of propagation, the thickness of the crystal also is another important condition.

Generally, to increase the doubling efficiency, a thicker crystal is preferred since there will be more medium where frequency-doubling can take place. However, for a thick crystal, only a narrow range of frequency can satisfy the phase-matching condition. If a pulse with frequency bandwidth larger than that narrow range, frequencies outside this small region doesn't get doubled. Hence if an intensity autocorrelation was done using this narrowed signal, the autocorrelation will lead to an overestimation due to the reduced frequency contributions.

SHG is the most widely used method of implementing intensity autocorrelations for pulses in the visible and near-infrared regions. However, due to

a lack of suitable non-linear crystals, implementation for pulses in the blue and ultraviolet regions are not readily available.

Two photon fluorescence

In two photon fluorescence, two photons gets absorbed simultaneously by a fluorophore exciting it. The fluorophore then fluoresces a photon at a certain wavelength due to spontaneous emission. The wavelength of the emitted photon is dependent of the fluorophore used. Detection of the fluorescence is similar to the second harmonic case.

Due to the nature of fluorophores, there are a wide variety of medium available across many frequency regions. However, due to difficulty in handling such media, it is only popular in the U-V region, where SHG implementations are not viable.

Two photon absorption

Similar to two photon fluorescence, two photons get absorbed by the medium in two photon absorption schemes. However, the medium doesn't have to be fluorescent. If it is assumed that there are no other losses other than two photon absorption, i.e. no single photon absorption can occur, then the intensity of transmitted light, I_{TRANSMIT}, would be

$$I_{\text{TRANSMIT}} = I_0 - I_{\text{TPA}}$$

where I_0 is the intensity of the beam before passing through the medium and I_{TPA} is the intensity of light absorbed due to two photon absorption. I_{TPA} would be the term holding the autocorrelation signal that we are interested in.

This can only occur when the medium that we are using is transparent at the frequency of the pulse we are interested in.

Another possibility in detecting the absorption of two photons is to look for the photoelectrons generated. This can only be done if the medium is conducting. What we are essentially looking for is a conductive material with high enough energy level spacings such that single photons do not get absorbed and hence do not generate photoelectrons. This sounds like a job for semiconductors which are band-gap materials. We shall take a look at them further in the next section.

2.2 Band-gap materials

A band-gap material has a valence and conduction band separated by a band-gap. At very low temperatures, the valence band is completely filled with electrons while the conduction band is completely empty of electrons. Without any free charge carriers, no current can flow through the material and it is non-conducting.

Charge carriers can be introduced by thermal or radiative excitation of an electron, which then can be detected as a current if an applied voltage is present. Hence, the current generated across a semiconductor is proportional to the number of excitations. Typically, radiative excitation, where a single photon of energy greater than the band gap is absorbed to excite an electron to the conduction band, is much more welcomed than electrons excited thermally in any light detection scheme. The photocurrent generated, $\mathcal{I}$ is proportional to the number of photoelectrons excited, N, which is then proportional to the intensity of light, I, falling on the semiconductor,

$$\mathcal{I} \propto N \propto I.$$

For photons with energy larger than the energy band-gap, this forms the basis of linear single photon detection. Additional structures like P-N junctions, Schottky barriers or avalanche regions may be built with the purpose of increasing the current generated for the same applied bias voltage.

It should be noted that in the linear detection region, absorption of photons with energy less than the energy band-gap of the semiconductor is very low. The photocurrent generated from these absorptions, mainly due to impurities present, are usually indistinguishable from the background noise due to thermal excitations. If we increase the intensity of light falling on the semiconductor, with photon energy still smaller than that of the band-gap, interesting things may start to happen as the detection starts to behave non-linearly.

With sufficient intensities, the probability of an electron being excited by two photons at the same time increases. Now,

$$\mathcal{I} \propto N \propto I^2.$$

The photocurrent generated is now dependent on the square of the intensity only, provided the current due to thermal excitations remains small.

An advantage of detection that is dependent on intensity only, rather than electric fields, is that we don't need to consider phase-matching or the polarisation of our light. Thus for two photon fluoroscence and absorption, we can simply shine light enough onto the medium to get a non-linear response. Since no phase-matching is required, the non-linear bandwidth of detection is determined only by the medium and thus can be very large.

Photosensitive diodes

The most commonly available semiconductor photodetector is the P-I-N junction silicon photodiode. It has a wide spectral absorption from mid UV up to the infrared region. For selective absorption from a narrow wavelength range, spectral filters are used such that only the wanted wavelengths reaches the photodiode, while the rest gets absorbed. This is unacceptable for non-linear detection since we need the semiconductor to be intrinsically to be able to absorb two photons directly. This won't happen if the lower energy photons are being absorbed by some other filter. As such, we need to need to find other semiconductor materials which are more suitable.

A non-obvious choice would be light emitting diodes. LEDs are made using various elements, depending on the colour of light needed, hence we have a wide selection of wavelengths to work with. Although some LEDs generate light across a wide spectrum and restricts their emission pattern by using coloured filters, most LEDs though have narrow intrinsic emission spectra. Hence it is prudent to assume that they have similarly narrow absorption spectra too.

Perhaps the most obvious of difference is that an LED needs a direct band-gap material while a silicon photodiode need no such constraint. A direct band-gap, in contrast with an indirect band-gap simply describes the relative position of the conduction band above the valence band. It is easier for electrons to be excited radiatively in a direct band-gap semiconductor than an indirect one. This is usually done by having a binary semiconductor, where more than one elements are present, instead of just single elements.

Chapter 3

Characterisation of LED

3.1 Design of typical LED

P-N junctions

The light emitting diode, LED, is a direct band gap semiconductor usually made from group III-V elements. It is a solid state device with a high electrical to optical power conversion efficiency. It typically functions using a P-N junction. Like in a normal diode, in the forward bias, current flows easily whilst in the reverse bias, there is very little current flow. The only difference however is that light is emitted in the forward bias for an LED due to electron-hole pair recombination in the junction. A typical current-voltage characteristics of a P-N junction is shown in figure 3.1. For operation in reverse bias, the amount of current flow is determined by the number of charge carriers present in the depleted region of the junction. Charge carriers, specifically electron hole pairs, can be generated either by thermal excitation or by radiative excitation through the absorption of a photon. Therefore, at constant temperature, the number of charge carriers present and hence the

reverse saturation current through the LED is proportional to the number of photons absorbed by the P-N junction.

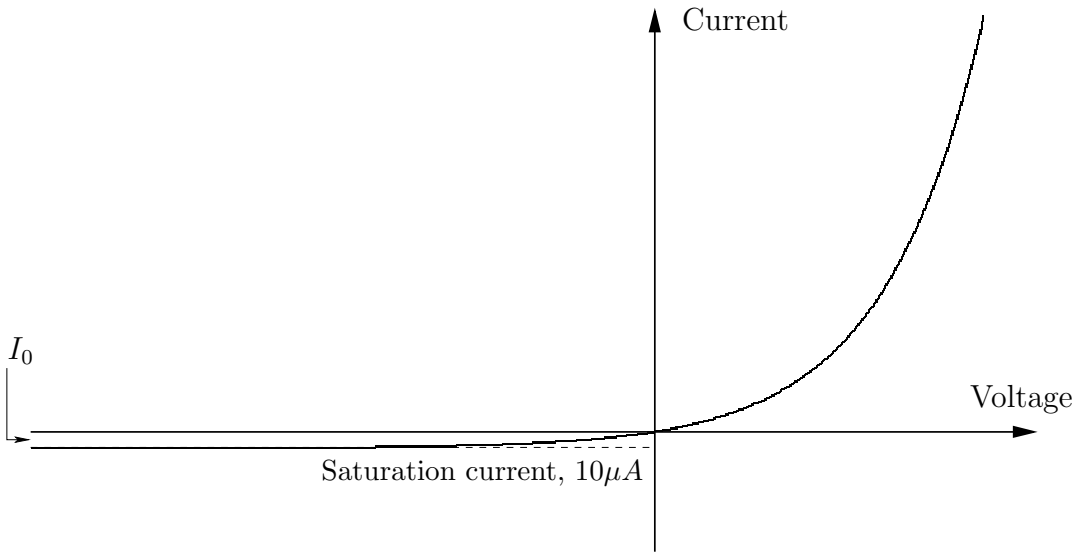

FIGURE 3.1: A typical current voltage characteristic of a P-N junction. In the forward bias, current increases exponentially with increasing voltage. In the reverse bias, current quickly saturates to saturation current, I_0.

A real LED

The LED comes in various shapes, sizes and colours. The two main uses for LED today are displays and lighting, and both have different usage requirements. Displays tend to require a high contrast ratio and a wide viewing angle while lighting sources require a high luminous efficacy and correct colour rendering. A common forward emitting LED is shown in figure 3.2. The light emitting chip has an area of about 100 μm^2 and is connected to the cathode directly and to the anode by a very low resistance thin wire, typically gold. This wire needs to be thin to minimise the amount of light blocked. All of

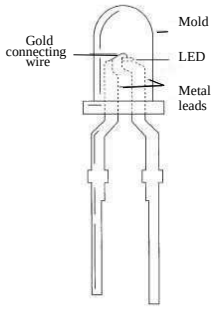

FIGURE 3.2: A schematic of a typical rounded 5mm forward emitting LED. The LED chip is usually placed in a reflector cup and encased in epoxy mold.

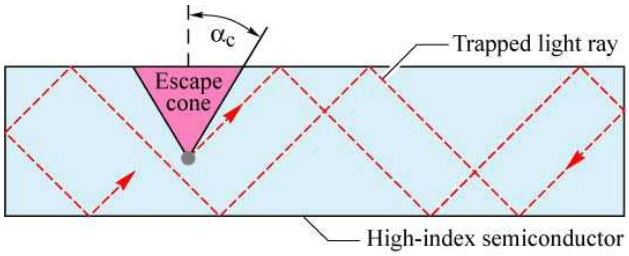

FIGURE 3.3: Light generated at an angle greater than α_c from the vertical is trapped inside the semiconductor by total internal reflection [10].

the light that is emitted comes from this very small layer of material and hence it is important that light extraction be efficient. A semiconductor has a high refractive index and total internal reflection at its interface with air causes only light generated within the escape cone to be able to escape the semiconductor. To increase extraction efficiency, a mold surrounds the LED and is made from epoxy having a refractive index higher than that of air, thereby allowing a larger light escape cone as shown in figure 3.4.

Reflectors are also present to reflect side emitted light such that most light

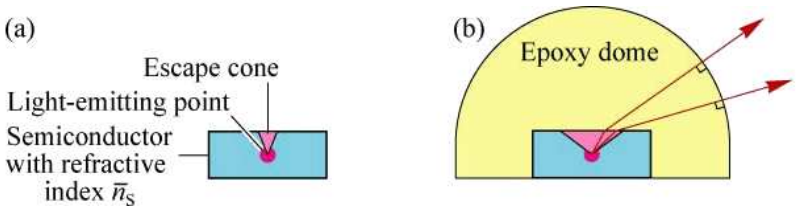

FIGURE 3.4: Light escape cone of a semiconductor (a) without epoxy mold and (b) with epoxy mold. The refractive index of epoxy, 1.4–1.8, gives a larger escape cone angle [10].

generated escapes through the top and not at the sides of the mold. Finally, if a domed mold is used, the spread or viewing angle of the light emitted can be controlled by choosing a suitable curvature of the mold which acts as a lens.

Colours of LED

Colour of the light emitted depends on the energy band gap of the P-N junction and hence is determined by the type of materials used. Gallium Arsenide is commonly used for red and Gallium Nitride for blue and green LEDs. Also, dopants, acceptor or donor impurities, can be introduced to slightly alter the wavelength of the light emitted to make, for example, yellow LEDs. The LED has a narrow emission spectrum of about 20–50 nm wide. Hence it is most likely that its absorption spectrum has a similar range as well. This narrow selectivity of wavelength is the main reason why we are using the LED as our detector. On comparison, the average photodiode has a typical response spectrum anywhere from 80 nm up to 2 µm.

3.2 LED as a current detector

The LED is inherently designed for emitting and not detecting light. Therefore it would be unreasonable to just hook it up to a ammeter and expect any significant current when we shine light on it. To get an idea of the order of magnitude of the current generated, we perform an estimate.

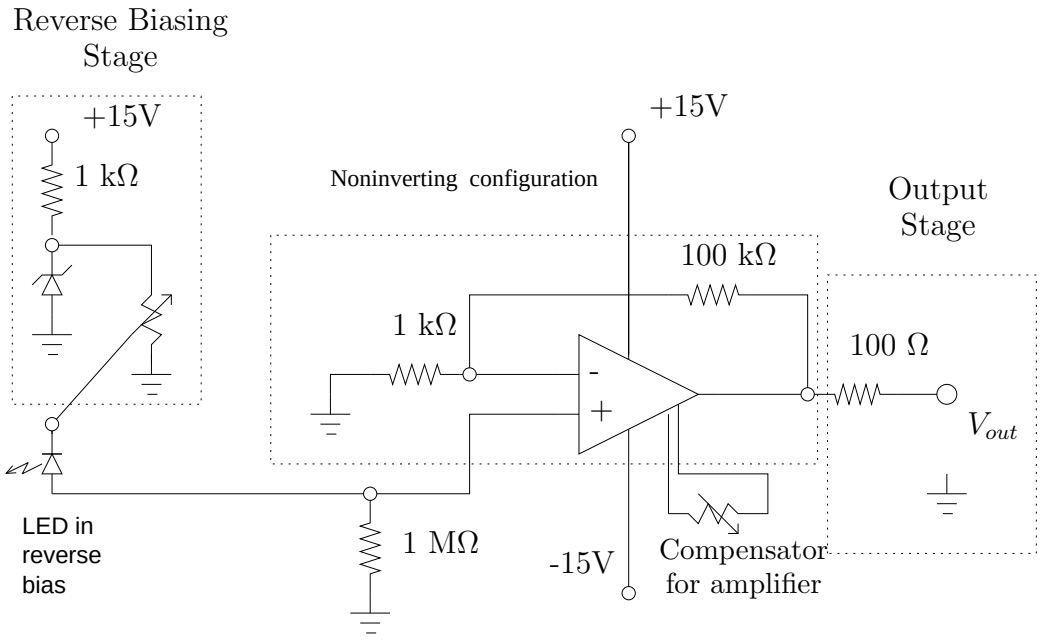

FIGURE 3.5: Circuit diagram of the current amplifier used for detecting photocurrent generated by an LED.

Referring to a data sheet, a current of 20 mA gives about 2000 millicandles of light which converts to an intensity of 3 mW. If we assume photocurrent generation has the same efficiency as light emission, we then get 7 A/W of optical power for single photon absorption. To find the flux, Φ, or the number of photons per second in 1 W of light, we use $P = \Phi hc/\lambda$. Using a typical wavelength of 600 nm, Φ equals 3×10^{18} photons per second. For two photons

transitions, we take the square root of Φ, since the probability of absorption is now dependent on the square of intensity now, getting an effective absorption of 2×10^9 photons per second. Converting back to optical power and again at 600 nm, this corresponds to 0.6 nW. Assuming that the same amount of current generated as in single photon absorption, we get, 4 nA for every watt of optical power, which is not detectable with an ordinary ammeter and requires some care to distinguish from noise. Hence we use a purposely built current amplifier (see figure 3.5). To safely transport the photocurrent generated to the amplification stage, a special shielded twisted pair cable, which picks up very little noise, is used.

3.3 Spectrum of LED

Since LEDs are not designed for light detection, their data sheets do not provide all the information that would simplify our task to select a particular device. Therefore we take the emission wavelength as a guide and acquired a collection of LEDs and tested them for their suitability. Table 3.1 lists the various LEDs acquired and their specifications quoted from their manufacturers. Since the absorption spectra of the LEDs cannot be easily measured, the emission spectra of the LEDs were taken instead [11] to ensure there are no other peaks other than the central maximum were present. Figure 3.6 shows their various spectrums. All are possible candidates for 2 photon absorption since the wavelength of the pulse we are working with is 780 nm and all fall below that value and above the half value of 390 nm.

Colour	Order-Code	Peak Wavelength, λ_0, [nm]	Spectral Halfwidth, [nm]
Red	301-5142	635	17
Amber	301-5051	592	17
Green	301-5245	524	47
Blue	301-5221	470	35

TABLE 3.1: List of LEDs obtained. LEDs are manufactured by Agilent Technologies and ordered through Farnell-In-One.

3.4 Non-linear response of LED

Although all are possible candidates for 2 photon absorption, how strong their non-linear response is with respect to intensity will determine which is the most suitable. To get a value for their non-linear response, we vary the intensity of light falling on the LED by using a half-wave plate and a polarising beam splitter and measure the photocurrent generated. Current response was taken in both continuous, CW, and pulsed mode. Due to the passive mode-locking of the laser system, CW operation can only reach around 500 mW before the laser switches to pulsed operation. As can be seen in figure 3.7, the non-linear response is much higher in pulsed operation. This is due to a higher peak intensity in a short pulse and hence a higher two photon absorption probability. Amber was found to have the highest second order non-linear coefficient and subsequently used in the setup of the autocorrelator.

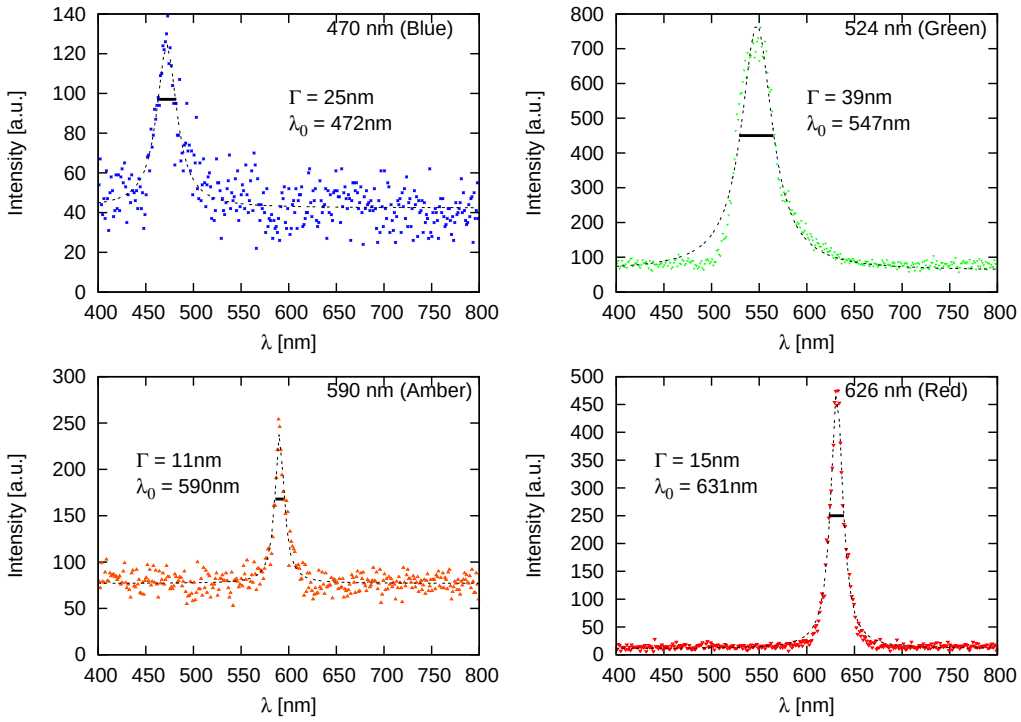

FIGURE 3.6: Spectrum of the various LEDs. Noise in the spectrum of the blue LED is due to inefficient collection of light in the spectrometer used. Spectra was fitted to a Lorentzian curve with full width half maximum, Γ.

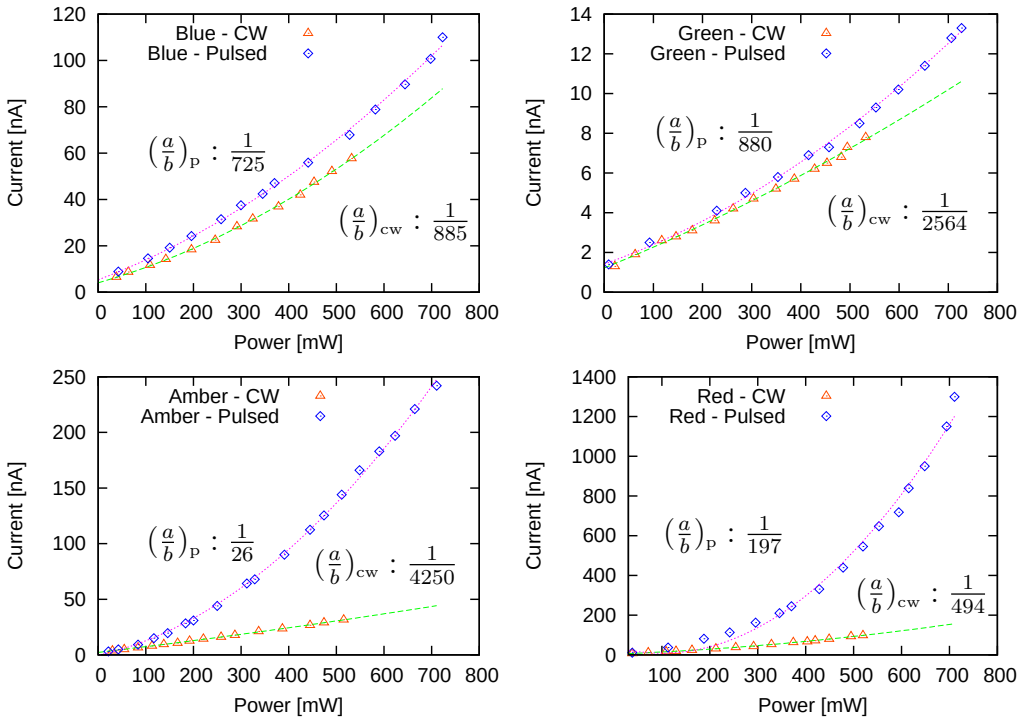

FIGURE 3.7: Non-linear response of current with increasing intensity of light on LED. It can be seen that opertation in the pulsed regime gives a much higher non-linear coefficient than in the continuous regime. $\frac{a}{b}$ gives the ratio of linear and second order coefficients from the best fit curve, where current, $I = aP^2 + bP + c$.

Chapter 4

Setup and results for a femtosecond pulse

4.1 Pulse dispersion in materials

There is a Fourier relation between time and frequency. A short pulse is made by mode-locking lots of different frequencies in phase, such that they interefere constructively for only a short time and destructively for all other times. As a result, the shorter a pulse, the more modes or frequency components it has. This means that a very short pulse essentially has lots of wavelength components and needs a medium that can amplify or lase at different frequencies. This is commonly refered to as bandwidth of the lasing medium. Table 4.1 lists common lasing medium, their bandwidth and the minimum pulse duration possible for each medium.

Travelling through a vacuum, the speed of light is c which is constant and equal for all wavelengths. When propogating through a normal medium however, the speed of light is dependent on the refractive index of the material, $n(\lambda)$, which is a function of wavelength. Hence, different wavelength com-

Lasing Medium	Bandwith [nm]	Shortest Pulse [fs]
Argon-Ion (520 nm)	~ 0.007	150,000
Ruby (694 nm)	~ 0.2	6,000
Nd:YAG (1064 nm)	~ 10	120
Dye (620 nm)	~ 100	12
Ti:Sapphire (800 nm)	~ 400	3

TABLE 4.1: Bandwidth of some lasers and the minimum pulse width they can generate.

ponents travel at different speeds through the material. This phenomenon is known as dispersion and what this means is that for a short pulse with a large bandwidth, pulse spreading will occur due to the difference in speeds.

Since some transmission through optical elements is inevitable, we should consider how much material we can tolerate before our pulse spread becomes comparable to the original width. From the specifications of our laser, we know the pulse that we are working with has a pulse width in the order of 100 fs. Also its peak wavelength, λ_0, is measured at 780 nm.

$$\lambda_0 = 780 \text{ nm} \quad \tau_p = 100 \text{ fs}.$$

Refractive index, $n(\lambda)$, as a function of wavelength, can be modelled by the Sellmeier equation,

$$\begin{aligned} n^2(\lambda) &= 1 + \frac{B_1\lambda^2}{\lambda^2 - C_1} + \frac{B_2\lambda^2}{\lambda^2 - C_2} + \frac{B_3\lambda^2}{\lambda^2 - C_3} \\ &= 1 + \sum_i \frac{B_i\lambda^2}{\lambda^2 - C_i} \end{aligned} \tag{4.1}$$

The Sellmeier coefficients of common optical glasses such as BK7, SF11 or fused silica, can be looked up Schott Glass catalogue. A plot of the refractive index of these materials are shown in figure 4.1.

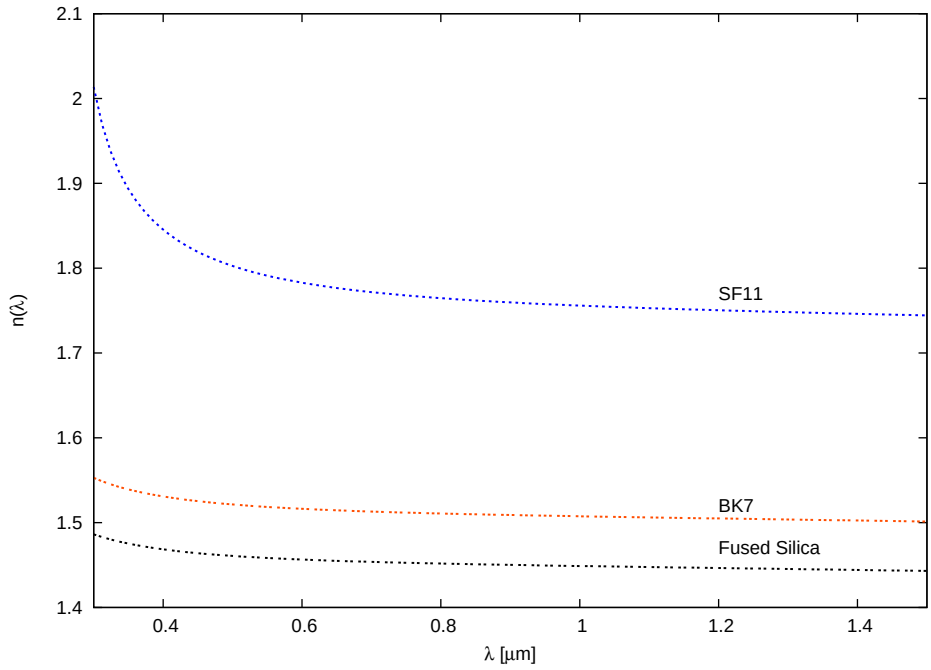

FIGURE 4.1: Refractive index of BK7, SF11 and fused silica at different wavelengths. Although they have different refractive index at 780 nm, they have relatively similar gradients at that wavelength resulting in similar pulse spreading for the same amount of material passed through.

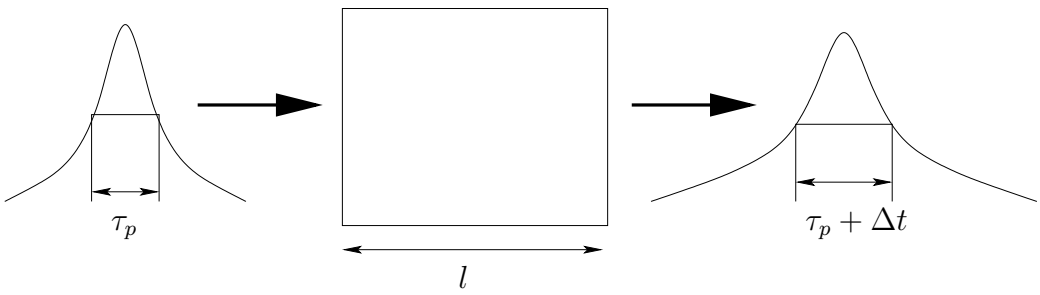

FIGURE 4.2: A pulse of width τ_p, spreads by Δt after passing through material of thickness, l.

The time taken, t of a pulse with velocity, v, to pass through a material of thickness, l, is related by, $t = l/v = l/nc$. For a fixed thickness, spread is then given by,

$$\begin{aligned} \Delta t &= \left| \frac{\partial t}{\partial n} \Delta n \right| \\ &= \frac{l}{n^2 c} \Delta n \\ \Rightarrow \frac{\Delta t}{l} &= \frac{\Delta n}{n^2 c} \end{aligned} \tag{4.2}$$

For a vacuum, Δn is zero and hence no pulse spreading occurs. For everything else, we find from equation 4.1,

$$\Delta n = n^{-1} \sum_i \frac{C_i B_i \lambda}{(\lambda^2 - C_i)^2} \Delta\lambda \tag{4.3}$$

For a Fourier limited pulse, the bandwidth, $\Delta\lambda$ can be calculated from its time-frequency product,

$$\frac{\tau_p \Delta\omega_p}{2\pi} = \tau_p \Delta\nu = \frac{\tau_p c \Delta\lambda}{\lambda^2} = K,$$

where K is a factor dependent on the shape of the pulse and $\nu = c/\lambda$. From table 1.1 on page 10, we have, $K = 0.315$, for a hyperbolic secant pulse shape. Putting all these in equation 4.2, we have,

$$\frac{\Delta t}{l} = \frac{K\lambda^2}{\tau c^2} \left[1 + \sum_i \frac{B_i \lambda}{\lambda^2 - C_i} \right]^{\frac{3}{2}} \Bigg/ \sum_j \frac{B_j C_j \lambda}{(\lambda^2 - C_j)^2} \tag{4.4}$$

For a 100fs pulse at 780 nm, table 4.2 lists the pulse spread per cm of glass. Unfortunately, the dispersion coefficients for the mold encasing the LED is not well characterised and so we are unsure how much spreading occurs within. To get a better approximate, it is possible to saw off the mold at the expense of optical transmission since the surface is no longer smooth. We will use these values to estimate the spread experienced by the pulse due to the autocorrelation setup.

Material	Spread [fs/cm]
BK7	1.54
SF11	3.26
Fused Silica	1.46

TABLE 4.2: Calculated pulse spreading of a 100fs pulse through some common optical glass.

4.2 Setup

For any autocorrelation setup, we need to combine the signal with an identical copy of itself. Therefore it is necessary that we first split the signal into two and then make the two copies overlap. Delay is introduced to one of the two signals by varying the distance travelled by the signal, which, for a constant velocity, just translates into a time delay. For an optical autocorrelator, this is achieved with an interferometric setup. It is particularly convenient to use a folded Mach-Zender interferometer, where corner cubes replace the mirrors used in a regular Michelson interferometer, because it avoids coupling of the beam back to the laser source. (See figure 4.3.) The whole setup is mounted onto a 10×10 inch breadboard which allows for easy relocation of the device to measure pulses of different lasers. We used BK7 glass for the optical elements and the total amount of glass passed through by the pulse is 3.5 cm, thus introducing a spread of about 6 fs for a pulse with an initial width of 100fs.

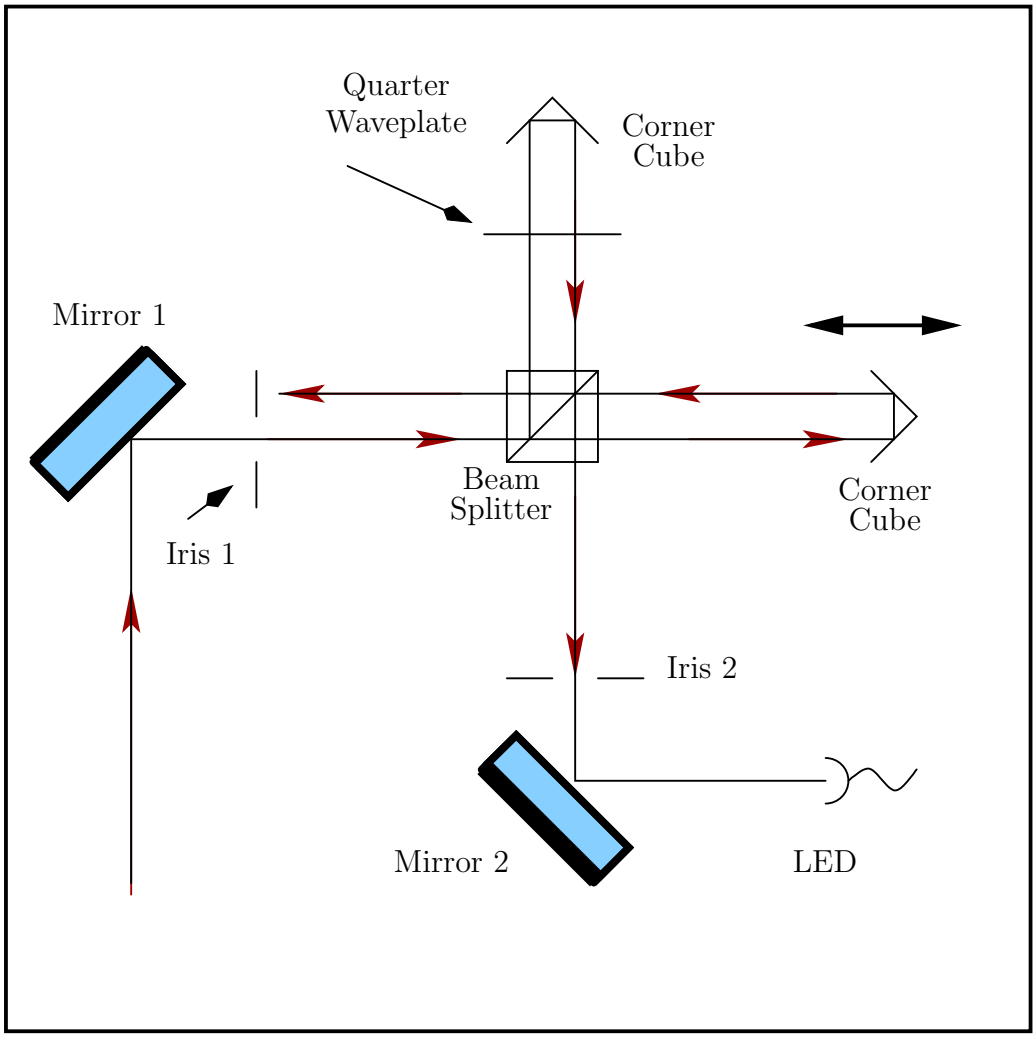

FIGURE 4.3: The whole setup is mounted on a small 10×10 inch breadboard. The irises and mirror 1 are used for aligning purposes. Iris 1 also acts as a beam dump for the second output. A quarter waveplate allows changing of the polarization of the fixed arm. Delay for the variable arm is done by placing the corner cube on a motorised translation stage.

Interferometric and non-interferometric autocorrelation

The pulse width can be found from either the intensity or interferometric autocorrelation. For an intensity autocorrelation however, there are no complicated fringe patterns making it easier to analyse over the interferometric kind. The drawback is that an intensity autocorrelation only has a contrast ratio of 3:1, as shown in section 1.2, making it more susceptible to any noise in the measurement.

Interferometric setups such as the one described typically leads to fringes at the output. In this case, we have to remove the fringes to obtain an intensity autocorrelation. This can be achieved via averaging of the fringes by using a numerical filter or by sweeping the delay fast enough such that the detection time is not able to resolve the fringes and thus averages it. Another way to get rid of interference is to have the two overlapping beams orthogonally polarised to each other. Since the LED does not need any phase matching conditions for its non-linear effect, only intensity, we can get an intensity autocorrelation even if the signals from the two arms do not interfere. This can be done by passing one of the beams through a half waveplate once. If the input is well defined and linearly polarised, then a half waveplate can rotate its polarisation by 90°. Due to the proximity of the folded beams though, a double pass through a quarter waveplate is more practical. A zeroth order waveplate with minimal thickness is used such that any extra spreading present in the fixed arm is negligible.

Measurement techniques

When the corner cube moves through a distance of x, the light pulse has to travel double that distance, $2x$. From displacement measurements, we have

$$\tau = 2x/c$$

where c is the speed of light in vacuum, 0.3 μm/fs. We scan our delay, τ, by at least twice the pulse width to get the full shape of the pulse. Measurements are done by taking current output of the LEDs as a function of x, after which we calculate the delay, giving the autocorrelation signal. It is assumed that the laser gives an output of identical pulses such that the autocorrelation can be constructed from these pulses for different delay.

4.3 Discussion

Intensity autocorrelation

When the quarter waveplate is rotated such that the beams in both arms are orthogonal, we have the intensity autocorrelation setup. An autocorrelation as in figure 4.4 is obtained.

It can be seen that there are still fringes present in the autocorrelation signal. This is most probably due to incomplete polarisation rotation by the quarter waveplate, leaving the beams still not completely orthogonally polarised. As such, further numerical averaging is needed before the autocorrelation width can be extracted. Also, it can be seen that the signal to background ratio is just 2:1 instead of 3:1 based on theoretical calculations. This is caused by non-perfect overlap of the two beams on the led and also a non-ideal 50:50 beam-splitter giving more contributions from one arm than

the other. We fit the autocorrelation signal to

$$\tilde{I}_2(\tau) \propto 1 + a\left\{6\frac{b\tau\cosh(b\tau) - \sinh(b\tau)}{\sinh^3(b\tau)}\right\} \tag{4.5}$$

from table 1.2, where a is to account for non-identical copies in both arms and $b = 2.72/\tau_{ac}$, and extract the autocorrelation FWHM, τ_{ac} as (196±3) fs. The actual pulse width, τ_p, is then obtained by dividing τ_{ac} by the deconvolution factor, k.

$$\tau_p = \frac{\tau_{ac}}{k} = (127 \pm 2)\text{fs}$$

where k is 1.543 for a hyperbolic secant squared pulse shape as listed in table 1.2. A pulse width of (127±2) fs is finally obtained. It should be noted that the error in the fit is less than that introduced by pulse spreading in the apparatus. However, we assume that the spreading experienced is a constant since all pulses pass through the same amount of glass each time.

Interferometric autocorrelation

If we rotate the quarter waveplate such that its fast axis is parallel to the electric field of the beam, no polarisation rotation will occur. Now the setup gives an interferometric autocorrelation and figure 4.5 shows the new autocorrelation signal.

Now, interference fringes are present in the autocorrelation signal. Although it is now technically more difficult to extract the pulse width, much more information is present. We have an increased signal to background ratio of 6:1 which is much bigger than that given by the intensity autocorrelation setup reducing errors due to noise fluctuations. It again does not reach the theoretical limit of 8:1 because of the beam overlap problem and non-ideal 50:50 beam-splitter used.

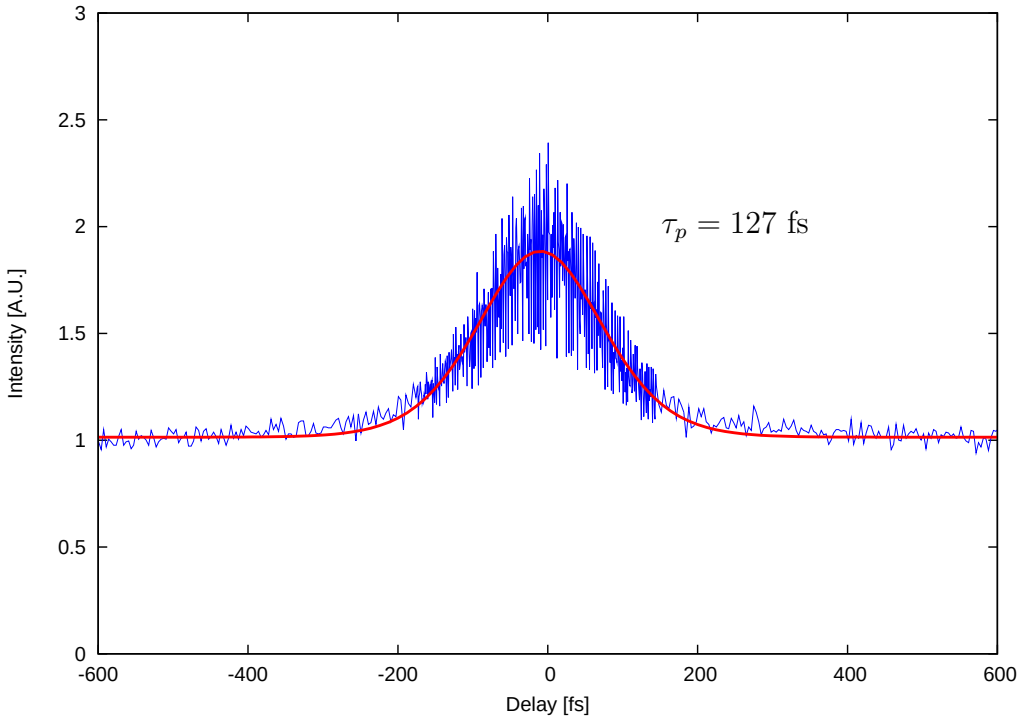

FIGURE 4.4: Intensity autocorrelation. Fringes are still present due to non-completely orthogonal electric field. Contrast ratio of signal against background is about 2:1.

Next we look at the autocorrelation signal envelopes. The fringes are between an upper and lower envelope, and the shape, length and beginning of these envelopes holds information about the pulse. For a relatively unchirped pulse[1], fringes are present at the wings of the autocorrelation and go all the way to background level. If some chirp is present, the fringes will begin at a point higher than the background level. In other words, the lower envelope will increase a little from background level before going to zero. From figure 4.5 it can be seen that a slight chirp is present in the autocorrelation which is caused by the dispersion introduced by the glass in the setup.

[1] An unchirped pulse is one that has a frequency that is constant in time.

It is also from these envelopes that we can extract the pulse width. This is done by extracting the autocorrelation signal edges and fitting them to

$$I_2(\tau) \propto 1 + c\left\{9\frac{d\tau\cosh(d\tau) - \sinh(d\tau)}{\sinh^3(d\tau)} \pm 3\frac{\sinh(2d\tau) - 2d\tau}{\sinh^3 d\tau}\right\} \qquad (4.6)$$

where c is to account for non-identical copies and $d = 2.72/\tau_{ac}$ again obtained from table 1.2. It should be noted that both the upper and lower envelopes theoretically have the same parameters and hence fitting either envelope to its function separately should yield the same parameters in both cases. The upper envelope has much more signal and hence it is easier to fit than the lower envelope.

An attempt to fit the upper envelope and subsequently checking that the parameters extracted give a reasonable lower envelope yields a pulse width of (130 ± 2) fs. As a check for consistency an intensity autocorrelation is extracted by numerically averaging the fringes revealing a pulse width of (141 ± 5) fs.

It is more difficult to determine the pulse width from the interferometric envelopes due to several reasons. The upper envelope increases rapidly making it harder for the fringes to reveal the true envelope due to limited resolution of the translation stage. Maximum constructive interference may not have been reached before a measurement is taken giving systematically lower values than the true upper envelope. The lower envelope does not decrease as rapidly and so the envelope is better revealed by the fringes. However, since the signal is close to zero, it is much more susceptible to noise.

Next, we look at the fringes present in the autocorrelation. If the measurement was performed again using smaller steps for the translation stage, fringes on the autocorrelation can be resolved. Figure 4.6 shows the details of these fringes. This fringes can provide a way of calibrating the delay. Since interference occurs every $n\lambda$ we can find out the scale of the delay by

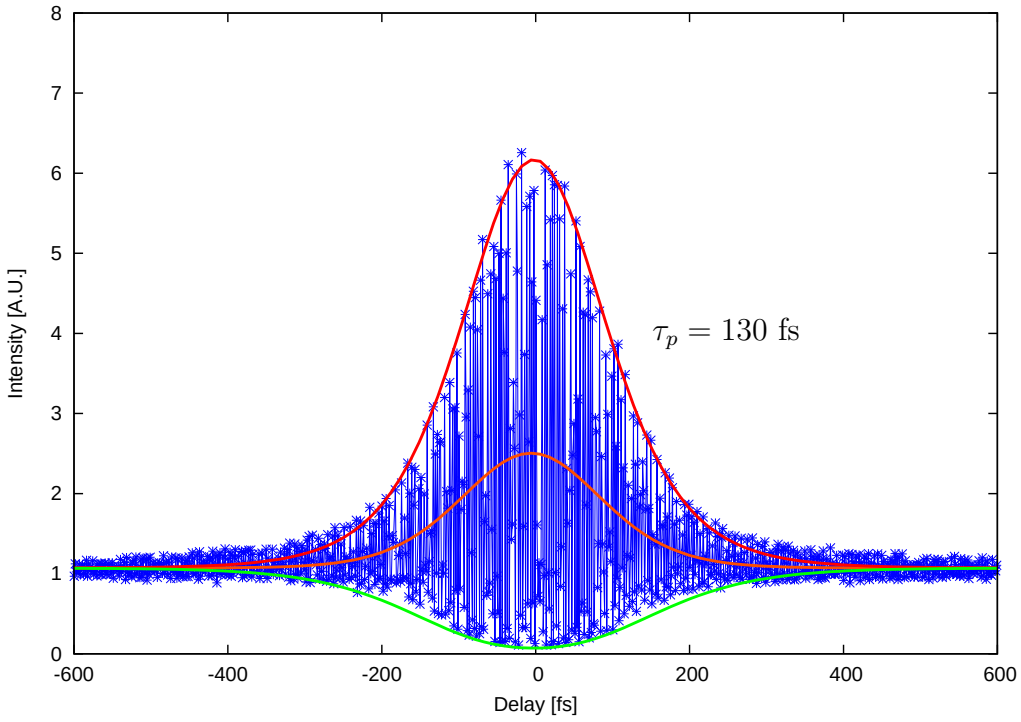

FIGURE 4.5: Interferometric autocorrelation of the earlier pulse in an interferometric setup. The autocorrelation full width half maximum can be extracted either by observation or using the equation of the best fit pulse envelope. Also, the averaged intensity is computed and its autocorrelation width extracted and compared.

counting fringes. For example, in figure 4.6, we count about 15 fringes giving,

$$n\lambda = 15 \cdot 780 \text{ nm} = 11.7 \text{ µm}.$$

The displacement measurement given by the motorised translation stage was 12 µm, which is quite close. However, resolution of the stage is not high resulting in jagged fringes instead of smooth sinusoidal ones. Also, at such small steps, the motorised translation stage is not able to move in linear steps but instead moves in jumps of large and small steps resulting in the

accordion-like fringes seen.

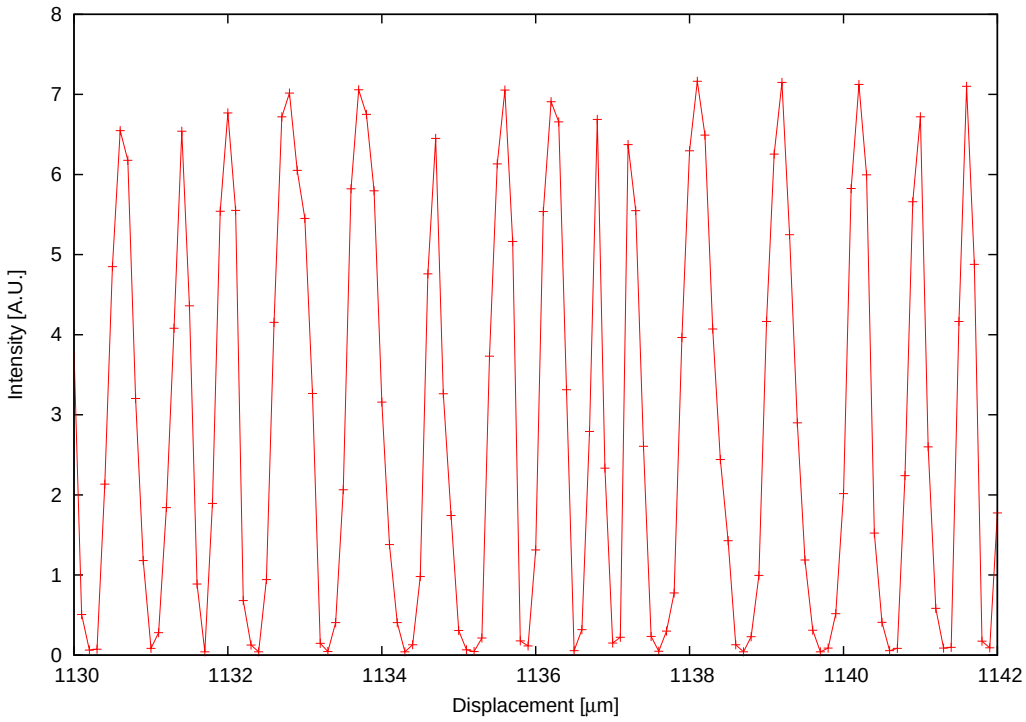

FIGURE 4.6: Fringes in the autocorrelation. There are 15 fringes for a displacement of 12μm.

Variable pulse widths

The mode-locked laser that we are using has tunable pulse widths. Since we can access pulses of different widths, we check the performance of our device. Because any shorter pulse would result in much more spreading than that that can be tolerated by our device, we perform measurements on longer pulses. Figure 4.7 shows the results of such measurements. To obtain a value for their pulse widths, fitting can be done to either the envelopes or the averaged intensity. In this case, the quoted pulse widths are done by

fitting the averaged intensity, since we have checked that both methods give results consistent with each other. Since the translation stage has a range of more than 5cm, we should be able to measure pulses of 100 ps or more. However, if the stage is displaced by such a large amount, alignment becomes even more important as the beams may gradually begin to lose their overlap, which becomes noticeable for large displacements.

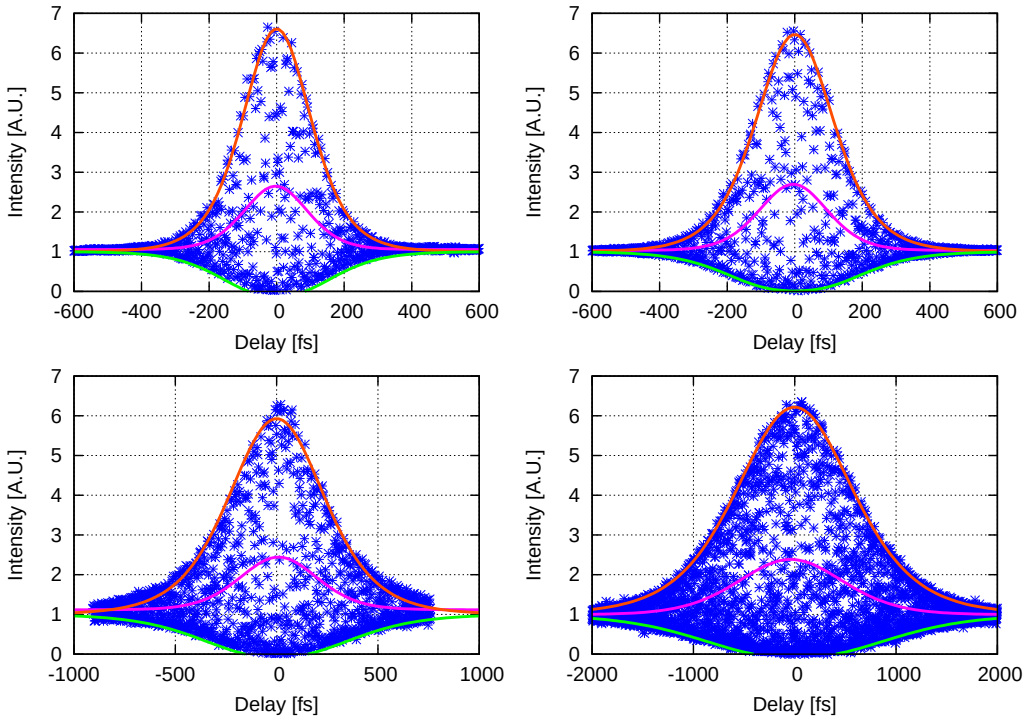

FIGURE 4.7: Autocorrelation of different pulse widths measured using interferometric autocorrelation setup. From left to right, top to bottom, the measured pulse widths are, 145, 155, 294 and 791 fs. Pulse widths are extracted from the numerically averaged intensity autocorrelation.

Pulse spreading through a fiber

To investigate how a pulse spreads through a dispersive medium, the light pulse was collimated into a 5 m, single-mode at 780 nm, fiber. Due to technical difficulties, the fiber wasn't placed before the input of the setup but between mirror 2 and the LED of figure 4.3. Without the fiber, the pulse was measured to have a width of 140 fs. The fiber is assumed to be made up of fused silica. Based on the calculations in section 4.1 we expect the pulse to be 0.88 ps long after passing through the fiber. Figure 4.8 shows the output measured using the interferometric autocorrelation setup.

There are three main features present in the autocorrelation. They are the spread of the autocorrelation, the intensity averaged part and the fringes present in the middle. The pulse width of the output is extracted from its averaged intensity, giving a value of 5.7 ps. This value is much greater than our estimate and hence we suspect other effects than dispersion.

A plausible explanation is the occurrence of non-linear effects. Since the pulse has to be collimated into the fiber by the use of a focusing lens, we expect an much higher intensity after focusing. This intense light will can lead to effects such as self-phase modulation (SPM), where new frequencies on either side of the peak frequency are created. This effectively causes a broadening of the frequency bandwidth. It should be noted that SPM by itself doesn't cause pulse spreading, only frequency broadening. However, when this new pulse passes through a dispersive medium, it will experience much more pulse spreading.

The fringes begins high up above the background level. This indicates a lot of chirp in the pulse. Interference occurs only for a small amount of delay, τ. Beyond this small delay, the two pulses are no longer within their coherence length giving an averaged-out intensity measurement. Within the

coherence length however, we can still see interference fringes, from which we can either calibrate the delay or make a make an estimate of the wavelength at which interference occurs. We count about 22.5 fringes in a delay of 60 fs. This corresponds to a wavelength of about 800 nm for the interfering light.

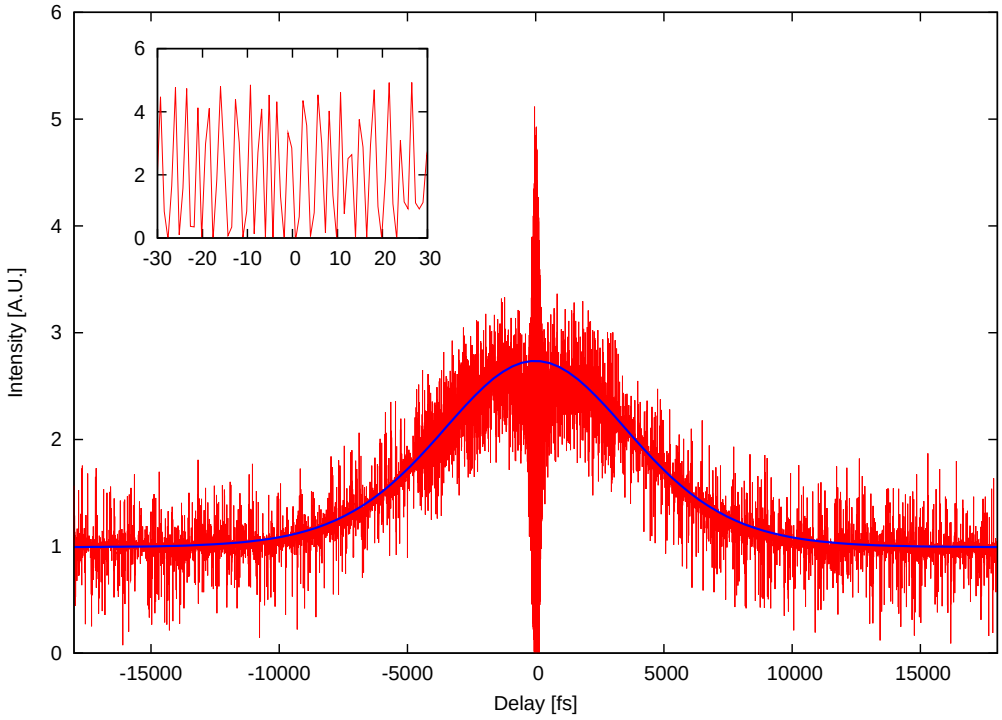

FIGURE 4.8: Autocorrelation of pulse after propagating through a 5m fiber. The presence of large noise is due to the low level of light collected at the output of the fiber.

To summarise, we see that the pulse has considerable chirp due to dispersion in the fiber, spreading is much more than that can be accounted for by only dispersion suggesting non-linear SPM effects. Only wavelengths a short bandwidth centered around zero delay can interfere. At larger delays, the phase mismatch of the different frequencies becomes larger, due to dispersion, and hence no more interference can occur.

Chapter 5

Conclusion and further work

We have built a compact and easy to operate optical autocorrelator for measuring ultrashort pulses in the near-infrared region. This was done using non-linear current detection in an LED instead of the usual SHG crystal and photomultiplier techniques. It can measure both interferometric and intensity autocorrelation signals.

The two forms of autocorrelation signals, was examined and the pulse width determined from each one, giving consistent results. Also further information about wavelength and chirp factor of the pulse can be obtained from the interferometric autocorrelation. Pulse measurements from 120 fs up to 6 ps was done demonstrating the range of our device.

Improvements

Dispersion in the autocorrelator is still significant for measurement of pulses less than 100 fs. Short of building a dispersion compensator, the next best way to reduce dispersion is to use as little glass as possible. Presently, the pulse has to pass through 3.5 cm of glass. This can be reduced by replac-

ing the corner cubes with right-angled mirrors. Furthermore, a half-silvered mirror can be used instead the beam-splitter cube, reducing the amount of glass used to a bare minimum.

Since the delay is done one step at a time by moving the translation stage and measuring the signal at that delay, obtaining the autocorrelation signal can be rather slow. If we are only interested in the intensity autocorrelation signal, we can replace the translation stage by a speaker. If we applied an AC voltage signal to the speaker, it will move back and forth, thereby sweeping through the entire delay much faster. However, interferometric autocorrelation signals are then not possible as the fringes are averaged since the detector is not fast enough to resolve them. Also, the delay range is limited by the amplitude and hence, the threshold voltage of the speaker.

What is next?

Since we are using an LED for non-linear detection, we can easily switch to LEDs of different colours to measure pulses at different wavelengths. One particular use is the measurement of pulses in the UV region (¡400 nm), obtained by frequency doubling a visible or near infrared pulse. This frequency doubled or upconverted source has important uses in the production of entangled states. However, most of the time, not much is known other than its spectrum and power. Hence a UV autocorrelator would be a nice way to know more about this upconverted source. UV LEDs are particularly expensive, so photodiodes built using binary semiconductor materials such as, Silicon Carbide or Gallium Nitride which are blind to photons at that wavelength, can be used instead.

If these UV photodiodes can detect a three photon absorption of 800 nm

photons with measurable current values, then we can exploit this third order non-linearity to do some cool stuff like triple correlators, where two different delay are used. Theoretically, phase information can be reconstructed from the measurements of a triple correlation [12], which would otherwise be unknown in a normal intensity autocorrelation.

Hence this choice of non-linear detection using band-gap materials gives us flexibility in our pulse measurements.

Bibliography

[1] L. Barry, P. Bollond, J. Dudley, J. Harvey, and R. Leonhardt, "Autocorrelation of ultrashort pulses at 1.5 μm based on nonlinear response of silicon photodiodes," *Electronics Letters*, vol. 32, pp. 1922–1923, September 1996.

[2] D. T. Reid, M. Padgett, C. McGowan, W. E. Sleat, and W. Sibbett, "Light-emitting diodes as measurement devices for femtosecond laser pulses," *Optics Letters*, vol. 22, pp. 233–235, February 1997.

[3] J. Diels and W. Rudolph, *Ultrashort Laser Pulse Phenomenon: Fundamentals, Techniques and Applications on a Femtosecond Time Scale*. Boston: Academic Press, 1996.

[4] C. Rullière, *Femtosecond laser pulses: principles and experiments*. New York: Springer Science+Business Media, 2005.

[5] V. Zakharov and A. B. Shabat, "Exact theory of two-dimensional self-focusing and one-dimensional self-modulation of wawves in nonlinear media," *Sov. Phys. JETP*, vol. 34, pp. 62–69, 1972.

[6] J.-C. M. Diels, J. J. Fontaine, I. C. McMichael, and F. Simoni, "Control and measurement of ultrashort pulse shapes (in amplitude and phase) with femtosecond accuracy," *Applied Optics*, vol. 24, 1985.

[7] P. A. Franken, A. E. Hill, C. W. Peters, and G. Weinreich, "Generation of optical harmonics," *Physcal Review Letter*, vol. 7, pp. 118–119, August 1961.

[8] M. H. R. Hutchinson, I. A. McIntyre, G. N. Gibson, and C. K. Rhodes, "Measurement of 248-nm, subpicosecond pulse durations by two-photon fluorescence of xenon excimers," *Optics Lettes*, vol. 12, p. 102, February 1987.

[9] J. I. Dadap, G. B. Focht, D. H. Reitze, and M. C. Downer, "Two-photon absorption in diamond and its application to ultraviolet femtosecond pulse-width measurement," *Optics Letters*, vol. 16, pp. 499–501, April 1991.

[10] E. F. Schubert, "Light emitting diodes and solid-state lighting." `http://www.lightemittingdiodes.org`; accessed 5th April, 2006.

[11] P. Y. Han, "Single photon sprectrometer," *NUS, Department of Physics*. UROPS project, 2006.

[12] J. Nicholas G. Paulter and A. K. Majumdar, "A new triple correlation technique for measuring ultrashort laser pulses," *Review of Scientific Instruments*, vol. 62, pp. 567–578, March 1991.

Appendix

Photograph of Autocorrelator Device

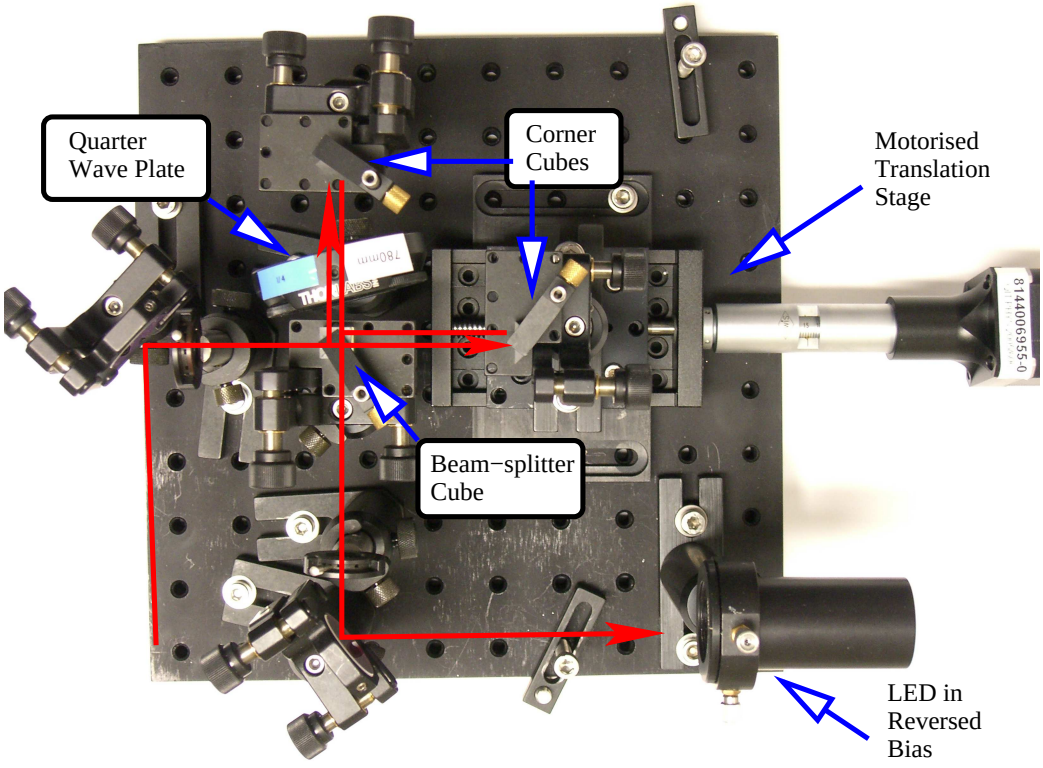

FIGURE 1: Top view of autocorrelator. The red arrow shows the direction of the beam.

List of equipments used

- Mode-locked Tsunami Ti:Sapphire femtosecond laser from Spectra Physics. Manufacturer specified peak output at 800 nm, and 100 fs pulses. Repetition rate of 80 MHz.
- OWIS stepper motor spindle on a translation stage. Specified with a resolution of 2 μm.
- High brightness AlInGaP LEDs from Agilent Technologies.